2019-11-01

Hydrodynamic X-Waves: Supplementary Material

James N. Steer[1], Alistair G. L. Borthwick[1], Miguel Onorato[2], Amin Chabchoub[3], Ton S. van den Bremer[4]
1. *School of Engineering, University of Edinburgh, Edinburgh EH9 3FB, UK.*
2. *Dipartimento di Fisica, Università di Torino and INFN, Sezione di Torino, Via Pietro Giuria 1, 10125 Torino, Italy.*
3. *Centre for Wind, Waves and Water, School of Civil Engineering, The University of Sydney, Sydney, NSW 2006, Australia.*
4. *Department of Engineering Science, University of Oxford, Oxford OX1 3PJ, UK*

LINEAR DISPERSION AND STABILITY

In our wavenumber spectrum, all non-zero components are confined to the lines $k_y = \pm(k_x - k_0)\tan\theta$, of which fig. S1a illustrates a positive arm at crossing angle θ. It is evident that the smallest value the frequency and wavenumber vector magnitude can take is given by $k_{\min} = k_0 \sin(\theta)$. Substituting $k_y = \pm(k_x - k_0)\tan\theta$ into the deep-water dispersion relation yields a result that is dependent on k_x only,

$$\omega = \sqrt{g}\left(k_x^2 + (k_0 - k_x)^2 \tan\theta^2\right)^{\frac{1}{4}}. \qquad \text{(S1)}$$

Figure S1b illustrates the group velocity $\mathrm{d}\,\omega/\,\mathrm{d}\,k_x$ obtained from (S1) for different crossing angles. It is evident that the optimum group velocity, which corresponds to no dispersion at leading order, occurs at the carrier wavenumber ($k_x/k_0 = 1$) for $\theta = \theta_c$. We note the similar behaviour of the lines corresponding to $\theta = 0°$ and $\theta = \theta_c^+/2$. The group velocity starts to deviate at larger and smaller wavenumbers, which would become significant in a more broad-banded spectrum.

The linear stability analysis of the uniform wave train solution to the 2D+1 NLSE perturbed by $a_\delta = a_{\delta,0}\exp(i\Omega t \pm [ik_x\,(x - c_g t) + ik_y y])$ gives for Ω [1, 2]

$$\Omega^2 = \frac{\omega_0^2}{8k_0^2}\left(\frac{k_x^2}{8k_0^2} - \frac{k_y^2}{4k_0^2} - k_0^2 A_0^2\right)\left(k_x^2 - 2k_y^2\right). \qquad \text{(S2)}$$

When Ω is imaginary and negative, the uniform wavetrain is unstable and grows (at rate $-i\Omega/c_g$ in space), as illustrated in fig. S2.

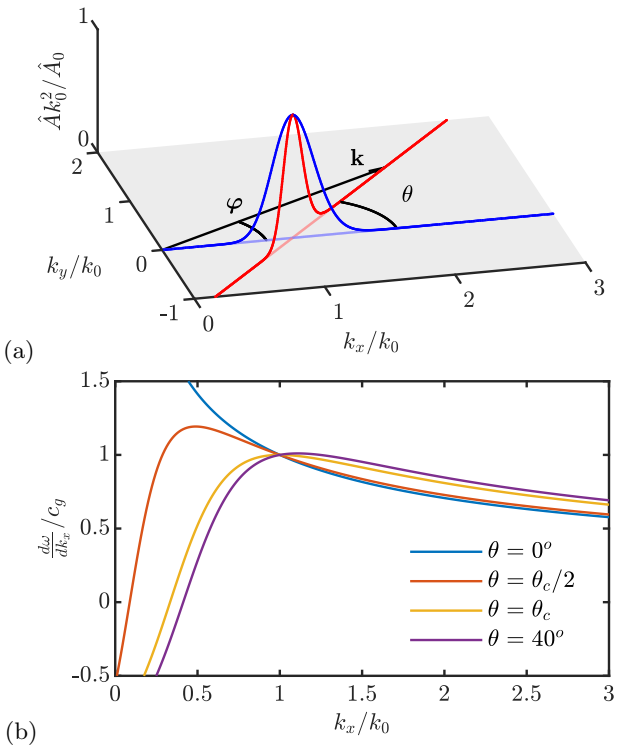

FIG. S1. Properties of the linear input spectrum: (a) amplitude spectrum for a crossed (red) and unidirectional (blue) wave group with wavenumber $\mathbf{k}$, crossing angle θ and component angle $\boldsymbol{\varphi}$, and (b) variation of the linear group velocity for the range of crossing angles θ studied experimentally in this paper.

EXPERIMENTAL METHODOLOGY

Facility

Figure S3 details the wave basin facility used for all experiments. Both actual wave gauges and effective wave gauges achieved with repeated experiments are shown.

Procedure

The generation of waves by the wavemakers is based on linear theory. Practically, constrained by the limited number of wave gauges available and their robust positioning, a total of 16 resistance-type wave probes were placed along a low gantry that spanned the tank in the x-direction. In certain experiments, the gantry was moved in the transverse direction to alter the measurement y-coordinate, giving the effective probe layout shown in fig. S3. The evolution of the X-wave was measured by recording the free surface elevation using 16 wave gauges spaced in 1.23 m increments along the x-axis from -9.5 m to 9.5 m (filled black circles in fig. S3), whereas the single crossed-wave experiments used 7 gauges spaced in roughly 2.5 m increments from -8.23 m to 4.42 m. All single crossed-wave experiments were repeated 4 times. For the X-wave, experiments were re-

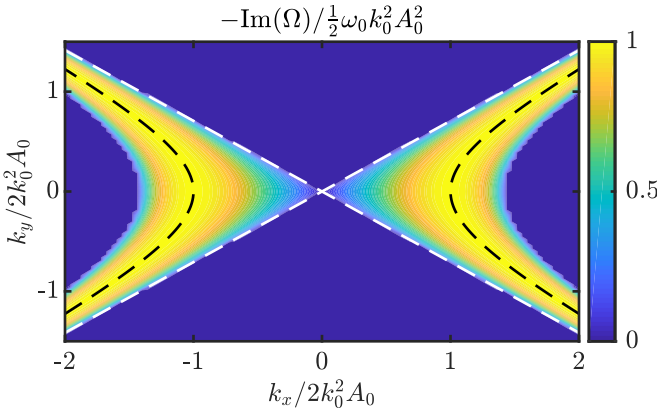

FIG. S2. Linear stability growth rate of the 2D+1 NLSE (from (S2)). The white dashed lines lie at the critical angles $\pm\theta_c$ and mark the angular boundary of stability. The black dashed lines mark the maximum growth rate contour.

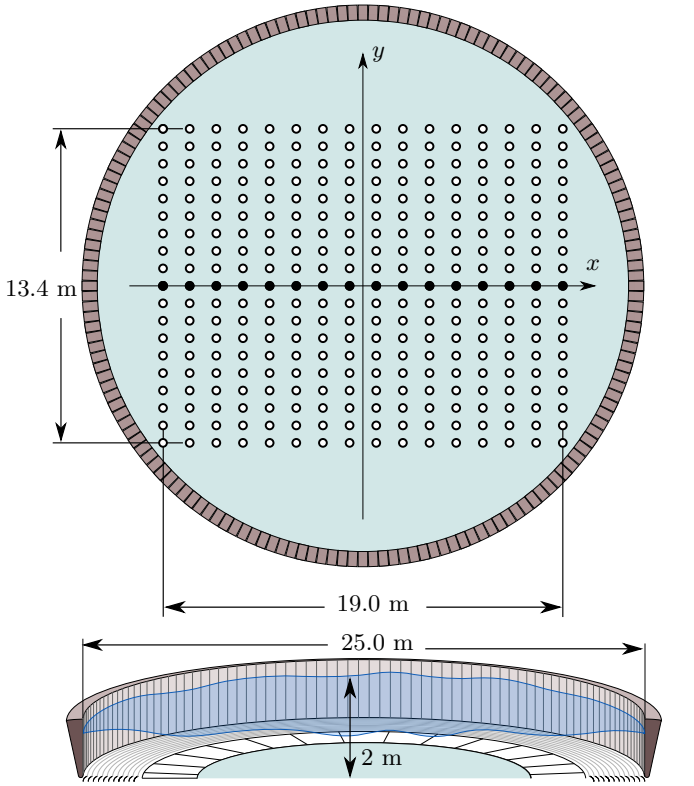

FIG. S3. Schematic of the FloWave basin: the filled circles indicate gauge positions during the single-crossed experiments and the open circles the effective gauge positions achieved with repeated experiments (adapted from [3]).

peated 19 times, moving the y-position of the gauges in 0.75 m increments in order to obtain the effective spatial array in fig S3. The wave gauges were calibrated at the start of each day of testing. A settling time of 20 min between each experiment was employed to allow for the absorption of reflected waves. In practice, the frequency vector was discretized such that each frequency was an integer multiple of $1/R$, where R is the repeat period of the test. All experiments were recorded for at least one repeat period with a sampling frequency of 128 Hz.

Data processing

In order to remove reflections, a 0.2-tapered Tukey window (25 s and 20 s for lower-steepness and higher-steepness experiments, respectively) was applied across the incident wave group free surface elevation time histories. For all experiments, amplitude spectra were estimated and treated using a band-pass frequency filter with lower bound $0.7\omega_0$ and upper bound $1.6\omega_0$ to remove noise, higher-order bound waves, and low-frequency bound waves. We centre the temporal signal about the time the group passes $x = 0$ ($t_{f,0}$) and normalize by the carrier period (T_0) and the intended linear focused amplitude at $x = y = 0$, A_0, which is not always generated to 100 % of the desired amplitude by the wavemakers, especially for the lower-steepness experiments.

FREE SURFACE ELEVATION TIME SERIES AND SPECTRA

Figure S4 shows examples of the band-pass filtered free surface elevation time histories recorded for expts. 1a and 2a (unidirectional) and 1c and 2c (θ_c^+) single crossed-wave groups at initial ($x = -5.7$ m) and final ($x = 4.4$ m) wave gauges. For the lower-steepness experiments, comparison between fig. S4a and b reveals distinct focusing over a distance of roughly 10 wavelengths in the unidirectional case (fig. S4a), whereas the group at the critical angle (fig. S4b) remains largely unchanged. This difference is more obvious for the higher-steepness experiments in fig. S4c,d, where dispersion and nonlinear amplitude growth are both suppressed at the critical angle. Spectra of the envelopes are shown in fig. S5 and discussed in the paper.

EXTENDED NUMERICAL SOLUTIONS

In order to determine the 'lifetime' of the coherent structures, an extended set of space-stepping numerical solutions were carried out at crossing angles $0° \leq \theta \leq 50°$ and steepness values $0.05 \leq \epsilon \leq 0.25$ for both single crossed and X-wave initial conditions. The percentage change in amplitude across a 17-wavelength (λ_0) evolution distance is presented in fig. S6, and the spatial 'lifetime' of the two crossed group structures is given in fig. S7. All single crossed-wave groups in fig. S6a show clearly the steady diminution of group velocity dispersion as the angle increases to the critical. The highest-

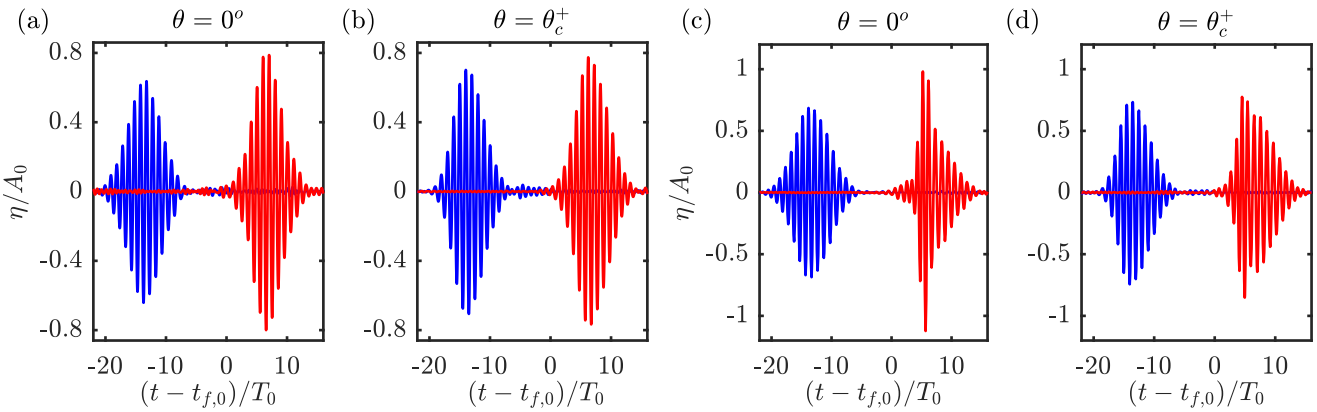

FIG. S4. Band-pass filtered free surface elevation time series (normalized by the carrier period, T_0) for the lower-steepness single crossed-wave expts. 1a and 1c (a,b) and the higher-steepness single crossed-wave expts. 2a and 2c (c,d). Blue and red lines present measurements from initial ($x/\lambda_0 = -6.67$) and final ($x/\lambda_0 = 3.60$) gauges, respectively. We centre the temporal signal about the time the group passes $x = 0$ ($t_{f,0}$).

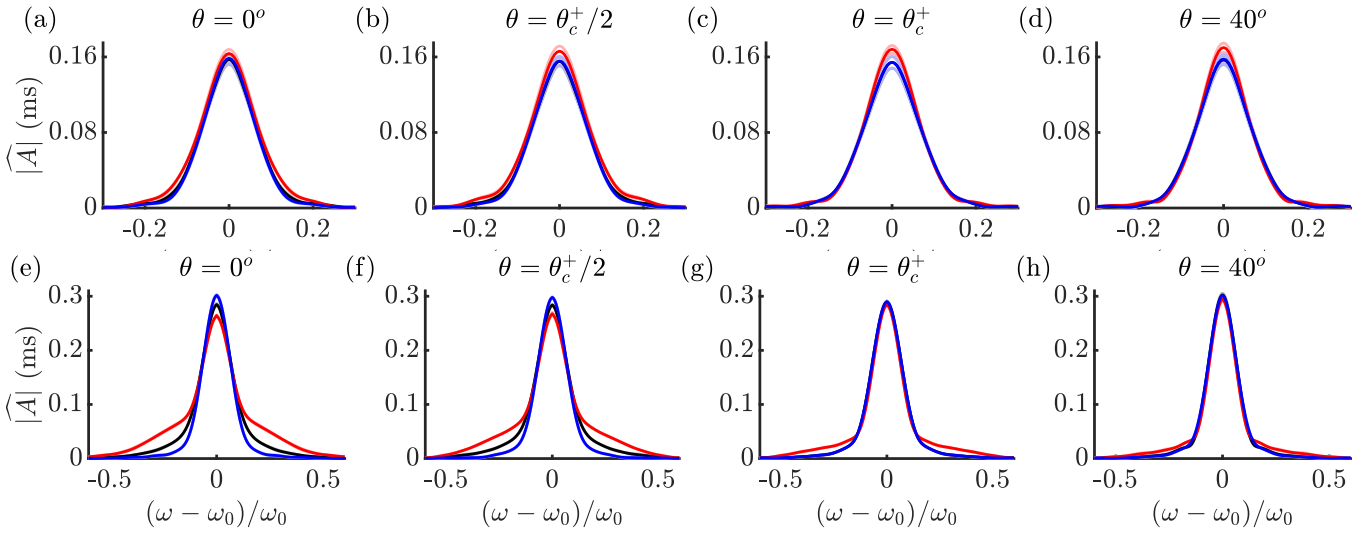

FIG. S5. Spectra of envelope time series in fig. 3, showing the lower-steepness expts. 1a-d (a-d) and the higher-steepness expts. 2a-d (e-h). Blue, red and black lines denote experiments at the initial ($x/\lambda_0 = -6.67$) gauge, and experiments and numerical solutions at the final ($x/\lambda_0 = 3.60$) gauge, respectively. The dark and light lines show the mean and the confidence bands (± one standard deviation).

steepness case in fig. S6a additionally shows an increase in amplification factor between $15° < \theta < 25°$, as reported in previous numerical [4] and experimental studies [5]. In fig. S6a, all wave groups show purely linear dispersion beyond the critical angle. The single crossed-wave group results are in slight contrast to the X-wave results presented in fig. S6b, whose critical angle shows sensitivity to nonlinear effects, increasing by up to 10° as groups become steeper. The lifetime estimates of single crossed-group structures presented in fig. S7a show a significant increase close to the critical angle and undetectable changes occurring at the critical angle for all steepness values, as is corroborated in fig. S6a. In the estimates of small-steepness X-wave lifetimes presented in fig. S7b, the critical angle is again seen to produce stationary structures. However, although the lifetime of every X-wave structure is increased at the 35.26° angle, in the higher-steepness X-wave cases of fig. S7b the angle of maximum longevity becomes sensitive to steepness and occurs at greater angles.

[1] H. C. Yuen and B. M. Lake, Nonlinear dynamics of deep-water gravity waves (Elsevier, 1982) pp. 67–229.
[2] P. G. Saffman and H. C. Yuen, Stability of a plane soliton to infinitesimal two-dimensional perturbations, Phys. Fluid. **21**, 1450 (1978).

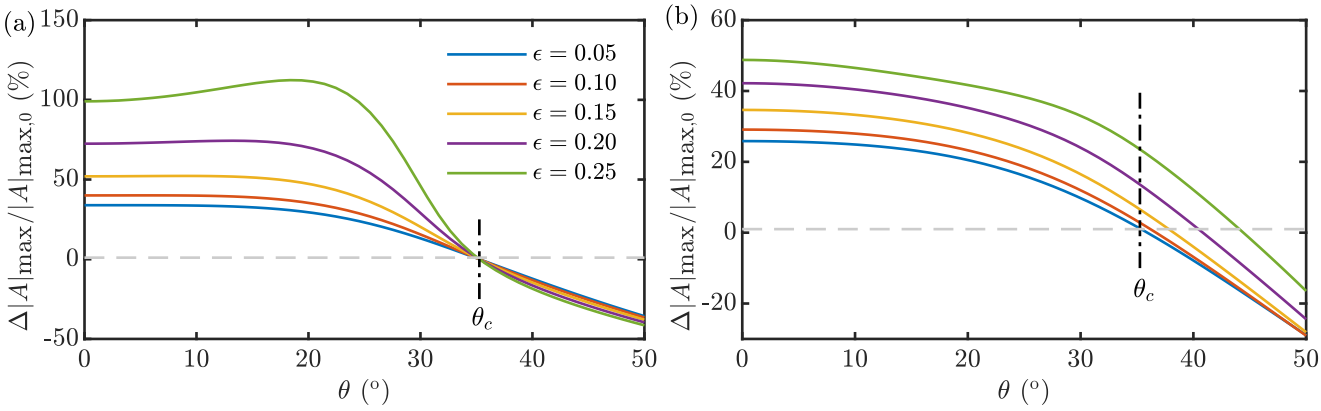

FIG. S6. Extended numerical solutions showing the percentage change in the maximum envelope amplitude, $|A|_{\text{max}}$ from the initial maximum amplitude $|A|_{\text{max},0}$ for single crossed (panel a) and X-wave (panel b) groups over an evolution distance of 17 wavelengths for different initial steepness values ϵ.

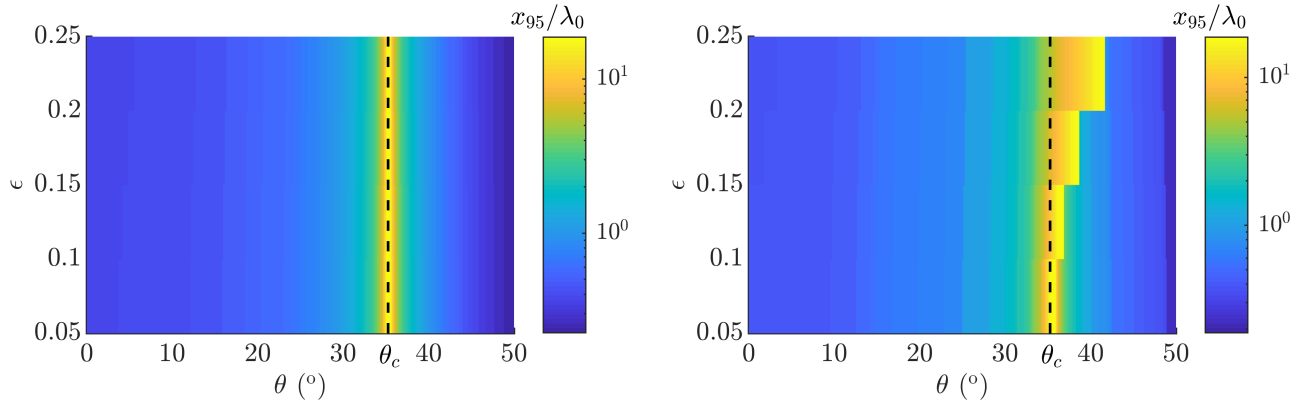

FIG. S7. Extended numerical solutions showing the number of wavelengths required for single crossed (panel a) and X-wave (panel b) maximum envelope amplitudes to change by ±1% for different initial steepness values ϵ.

[3] D. R. Noble, Combined wave-current scale model testing at flowave, EngD (2017).
[4] E. B.-G. K. T. Gramstad, O. and J. N. Borge, Modulational instability and rogue waves in crossing sea states, J. Phys. Oceanogr. **48**, 1317 (2018).
[5] A. Toffoli, E. M. Bitner-Gregersen, A. R. Osborne, M. Serio, J. Monbaliu, and M. Onorato, Extreme waves in random crossing seas: Laboratory experiments and numerical simulations, Geophys. Res. Lett. **38** (2011).